Applied Mathematical Modelling 67 (2019) 219–233

Contents lists available at ScienceDirect

Applied Mathematical Modelling

journal homepage: www.elsevier.com/locate/apm

A 3-D coupled Smoothed Particle Hydrodynamics and Coarse-Grained model to simulate drying mechanisms of small cell aggregates

C.M. Rathnayaka[a,b,*], H.C.P. Karunasena[c], W. Senadeera[d], H.N. Polwaththe-Gallage[a], Y.T. Gu[a]

[a] Queensland University of Technology (QUT), Science and Engineering Faculty, School of Chemistry Physics and Mechanical Engineering, Brisbane, Australia
[b] Department of Chemical and Process Engineering, Faculty of Engineering, University of Moratuwa, Moratuwa, Sri Lanka
[c] Department of Mechanical and Manufacturing Engineering, Faculty of Engineering, University of Ruhuna, Hapugala, Galle, Sri Lanka
[d] School of Mechanical and Electrical Engineering, University of Southern Queensland, Springfield, Australia

ARTICLE INFO

Article history:
Received 30 April 2017
Revised 5 September 2018
Accepted 17 September 2018
Available online 29 October 2018

Keywords:
Meshfree methods
Plant cell morphological changes
Smoothed Particle Hydrodynamics (SPH)
Coarse-Grained (CG) methods
Computational mechanics: Food drying

ABSTRACT

Recently, meshfree-based computational modelling approaches have become popular in modelling biological phenomena due to their superior ability to simulate large deformations, multiphase phenomena and complex physics compared to the conventional grid-based methods. In this article, small plant cell aggregates were simulated using a three dimensional (3-D) Smoothed Particle Hydrodynamics (SPH) and Coarse-Grained (CG) coupled computational approach to predict the morphological behaviour during drying. The model predictions of these cell aggregate models have been compared qualitatively and quantitatively through comparisons with experimental findings. The results show that the shrinkage and wrinkling behaviour of cell cluster models are in fairly good agreement with real cellular structures. The agreement between the cell aggregate model predictions and the experimental findings are closer in the high and medium moisture content values ($X/X_0 \geq 0.3$), than highly dried stages ($X/X_0 < 0.3$). Further, optimisation and sensitivity studies have been conducted on model parameters such as particle resolution, smoothing length, mass transfer characteristics and wall forces. Overall, the 3-D nature of this model allows it to predict real 3-D morphological changes more realistically compared to the previous meshfree based 2-D cellular drying models. The proposed 3-D modelling approach has a higher potential to be used to model larger plant tissues with complicated physical and mechanical interactions as well as their multiscale interactions.

1. Introduction

In numerical modelling of cellular structure, grid-based (or mesh-based) methods and meshfree methods are the two main techniques which have been used in the context of food engineering research so far. Grid-based numerical techniques such as Finite Element Method (FEM), Finite Difference Method (FDM) and Finite Volume Method (FVM) have been widely

* Corresponding author at: School of Chemistry Physics and Mechanical Engineering, Science and Engineering Faculty, Queensland University of Technology, 2 George Street, Brisbane QLD, 4001 Australia.
E-mail address: charith.rathnayaka@qut.edu.au (C.M. Rathnayaka).

https://doi.org/10.1016/j.apm.2018.09.037
0307-904X/

used and there is commercial software being developed for this purpose [1–3]. Despite their success, there are significant limitations in their ability to perform effectively and efficiently in the situations with large deformations, multiphase phenomena, free surfaces, moving boundaries and dynamic interfaces [4–7]. This is because the 'grid' or 'mesh' based methods result in lower accuracy and higher computational cost particularly when treating such complicated phenomena [8–13]. In order to overcome 'grid-based' deficiencies, meshfree (or grid-free) numerical methods have been developed [7,14]. In meshfree methods, a pre-defined mesh is not involved to discretise the problem domain. Instead, arbitrarily distributed nodes or particles are used, which are not interconnected permanently, and their neighbourhood is not fixed [15,16]. Meshfree methods have proven to be stable when dealing with complex physical phenomena such as large deformations, multiphase interactions and multiscale physics. A variety of meshfree methods has been developed so far [17,18].

Recently, there have been several "first generation" efforts to numerically model plant cells and tissues with the use of a coupled Smoothed Particle Hydrodynamics (SPH) and Discrete Element Method (DEM) approach, particularly targeting macro and micro mechanics of fresh (undried) cellular matter [12,19–21]. Based on those models, the "second-generation" of SPH-DEM coupled models have also been developed, which can simulate both fresh and dried cellular morphological changes of individual plant cells [22,23] and cell aggregates [12,24–28]. However, because these "second generation" investigations had only focused on the two-dimensional (2-D) mechanisms, a "third generation" study was carried out and published by us previously [16,29]. The main objective there was to computationally investigate the realistic three-dimensional (3-D) cellular structures [30]. In that "third generation" study, a coupled SPH and CG computational modelling approach was developed to model 3-D single plant cells during drying [16]. The focus was on the initial development aspects of the 3-D SPH-CG approach and application of that approach to simulate different categories of single plant cells.

In this article, we have developed multiple-cell 3-D SPH-CG computational models, where a novel computational strategy has been used to simulate three-dimensional (3-D) two-cell and four-cell aggregates which can be used to model the morphological behaviour of small plant cell aggregates during drying processes. To elaborate the significance of studying the cell aggregates than individual cells, the model predictions of this work were compared with single cell models. Further, the sensitivity of the model performance has been evaluated under a number of crucial physical and numerical parameters. For example, in this article, we discuss how the performance of the simulations are affected by varying mass transfer characteristics, wall contraction force-fields and wall bending force-fields. Additionally, we computationally evaluate the optimum SPH smoothing length and particle resolution in order to guarantee a higher model accuracy. These details are presented in the sections below.

2. Methodology

2.1. Particle representation of a cell in three-dimensions (3-D)

Plant tissues are made out of different categories of cells, each serving a unique purpose, while in collaboration with each other, in a given plant structure. Since parenchyma cells are the major contributor for tissues in a given plant [31], this study focused on numerically modelling single parenchyma cells and their small aggregates. Here, the original basic shape of an undeformed single cell was taken as spherical (see Fig. 1) [9]. Similar to our previously published study [16], a cell was assumed to be mainly consisting of the cell fluid and the cell wall while a coupled Smoothed Particle Hydrodynamics (SPH) and Coarse-Grained (CG) computational framework was used for modelling. Accordingly, the mechanical stresses developed in the cell wall are balanced by the pressure forces exerted by the expanding (or contracting) cell fluid in accordance with the Young-Laplace Law [2,9,11,22,31,32]. During cellular deformations, the cell wall is either stretched or contracted and in return, the cell fluid volume gets deformed. Here, the fluid and wall domains were discretised as given in Fig. 1, following basic principles of SPH and CG [13,16,17,33,34].

Different types of forces derived through relevant fundamental physical relationships were utilised to estimate particle properties and interactions among fluid and wall particles. As this work is an extension of our previous work [16] , only the novel computational model developments are presented and discussed in detail in this article.

2.2. Cell fluid model

Generally, the content of water in cell cytoplasm is about 80–90% [21] and accordingly, cell fluid was approximated to an incompressible homogeneous Newtonian liquid with properties similar to water. This facilitated modelling the fluid dynamic behaviour of the cell fluid using Navier–Stokes equations [35,36]. At the same time, cell fluid viscosity has been assumed to be higher than water to comply with viscous cell fluid characteristics. Low-Reynolds number fluid characteristics were assumed to represent the stagnant fluid nature in a cell. This low-Reynolds number viscous flow characteristics could effectively be modelled by a customised SPH framework [16,22,28,37]. As observed from Fig. 2, the cell fluid was modelled with a combination of four types of force fields as discussed in our previous work [16]: pressure forces ($\boldsymbol{F^p}$), viscous forces ($\boldsymbol{F^v}$), wall-fluid repulsion forces ($\boldsymbol{F^{rw}}$) and wall-fluid attraction forces ($\boldsymbol{F^a}$). Accordingly, the total force $\boldsymbol{F_i}$ on any fluid particle i could be defined as shown in Eq. (1). (see our previously published work [16] for details).

$$\boldsymbol{F_i} = \boldsymbol{F_{ii'}^p} + \boldsymbol{F_{ii'}^v} + \boldsymbol{F_{ik}^{rw}} + \boldsymbol{F_{ik}^a} \tag{1}$$

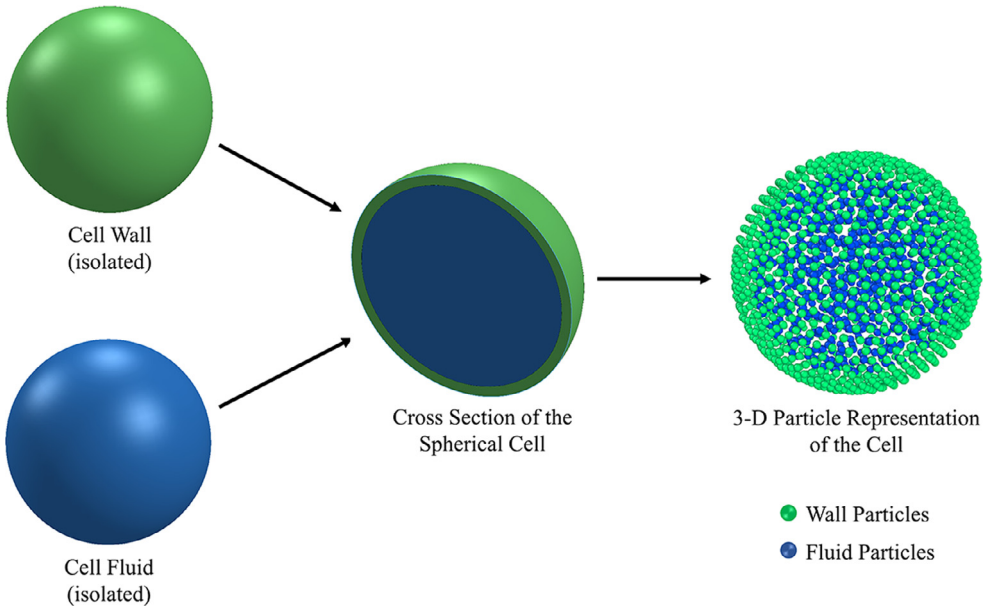

Fig. 1. 3-D particle representation of a single cell model, consisting of two main model components: cell fluid and cell wall [16]. Reproduced with the permission from Royal Society of Chemistry.

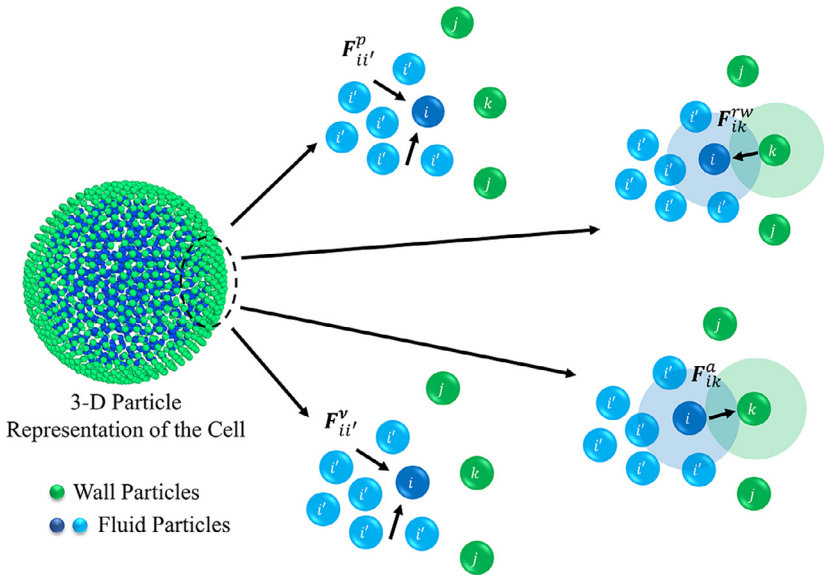

Fig. 2. Force fields in the 3-D SPH fluid model: pressure forces (F^{p}), viscous forces (F^{v}), wall-fluid repulsion forces (F^{rw}) and wall-fluid attraction forces (F^{a}) [16]. Reproduced with the permission from Royal Society of Chemistry.

2.3. Cell wall model

Plant cell walls play a crucial role towards the overall morphological behaviour of plants and their tissue structures. Biopolymers such as pectin, cellulose and hemicellulose contribute to the majority of the plant cell wall content as base materials [38–40]. Thin structures made out of these biopolymers establish the mechanical integrity of a plant cell. Such a complex cell wall structure cannot be simply modelled with a linear elastic stress-strain relationship as the cell wall material demonstrates time dependent hybrid elastic-plastic characteristics [16,21,41]. Within this context, a Coarse-Grained (CG) approach was used to numerically discretise the wall section of this model. As seen in Fig. 3, the network of CG particles that represent the cell wall were placed in a hollow-spherical geometry with local inter-links. It was treated as a particle scheme which consists of interconnected representative particles which are bonded as a network. Each element possesses the characteristics of the analogous wall element. The changes of morphology are characterised by the movement

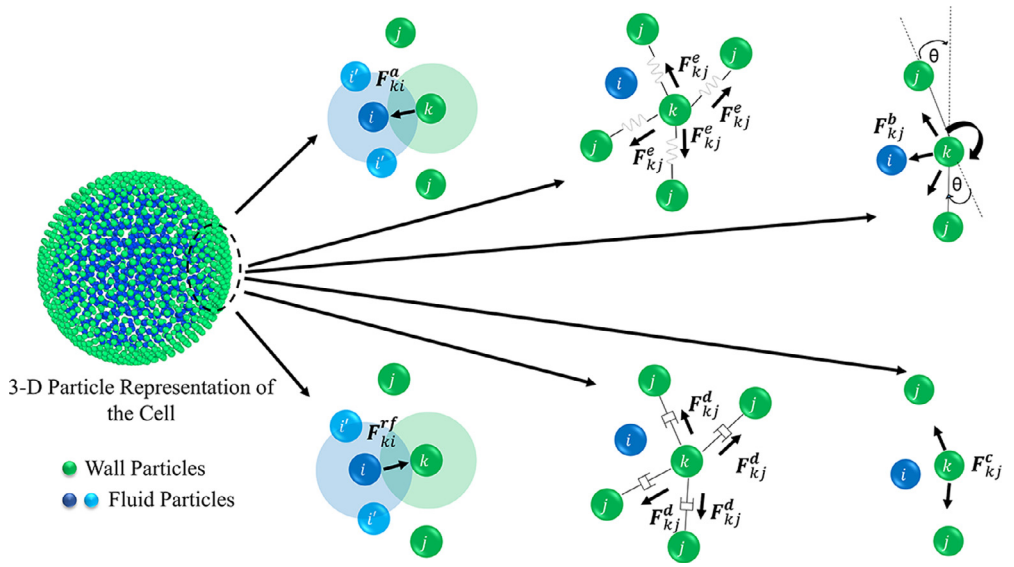

Fig. 3. Force fields in the Coarse-Grained (CG) 3-D wall model: stiff forces (F^e), damping forces (F^d), wall-fluid repulsion forces (F^{rf}), wall-fluid attraction forces (F^a), bending stiffness forces (F^b) and wall contraction forces (F^c) [16]. Reproduced with the permission from Royal Society of Chemistry.

of particles through six types of force interactions [16]: stiff forces (derived from harmonic potential) (F^e), damping forces (F^d), wall-fluid particle repulsion forces (F^{rf}), wall-fluid particle attraction forces (F^a), bending stiffness forces (F^b) and wall contraction forces (F^c) as illustrated in Fig. 3 [16,22,23,28]. Accordingly, the total force (F_k) on a wall particle k will be derived as in Eq. (2). (see our previously published work [16] for details).

$$F_k = F^e_{kj} + F^d_{kj} + F^{rf}_{ki} + F^a_{ki} + F^b_{kj} + F^c_{kj} \tag{2}$$

2.4. Modelling cell aggregates

In literature, Van Liedekerke et al., in their "first generation" approaches, have developed a simple and easy to implement tissue model by aggregating SPH-DEM based individual cells to study the mechanical response of fresh plant tissues under mechanical loading [19,20]. However, there are some conceptual and numerical limitations of this approach [28]. Firstly, their cell aggregation method does not consider the thickness of the middle lamella. The model is configured with neighbouring cells having coinciding cell walls even though they have hypothetically incorporated a middle lamella effect by using a stiff force interaction among cell-cell contacts. According to this hypothesis, the resulting steady-state multi-cellular system has coinciding adjacent cell walls which is not quite realistic. Furthermore, they have used Lennard-Jones (LJ) type repulsion forces to avoid cell-cell penetrations in a computationally expensive manner [28].

Karunasena et al., in their "second generation" approaches, have adopted a similar methodology with significant improvements in order to develop a two-dimensional (2-D) multiple-cell (small tissue) model to study tissue drying [27,28]. They incorporated a positive gap between adjacent cells to resemble the middle lamella found in real tissues. Similar to Van Liedekerke et al.'s work, they used two types of force interactions to demonstrate the interactions among cells in a multiple-cell arrangement: stiff forces due to the pectic materials in the middle lamella and LJ repulsion forces in order to prevent intra-penetrations among neighbouring cells. However, in the cell-cell LJ repulsion force interactions, the cells are repulsed only using the cell wall particle network unlike in Van Liedekerke et al.'s work, where the full array of fluid particles are used. Considering the computational cost of SPH-DEM computations, the approach of Karunasena et al. appears to be more computationally efficient [22,28].

Considering the positive outcomes produced by the above mentioned small-tissue developing methodologies, a similar approach was adopte to develop our 3-D small-tissue scale drying model in our "third-generation" investigations. This methodology can be simply represented as given in Fig. 4. As shown in Fig. 4(a) and (b), the cells are initially set as spheres and a positive initial gap is placed between neighbouring cells in order to represent the middle lamella observed in real plant tissues. As depicted in Fig. 4(c) and (d), the interactions among cells have been defined using two force interactions: stiff forces due to the pectic materials in the middle lamella and LJ repulsion forces in order to prevent intra-penetrations among neighbouring cells. The pectin layer stiff forces have been defined using a linear spring model between adjacent wall particles similar to Karunasena et al.'s and Van Liedekerke et al.'s works (see Fig. 4(c)) [20,28]. When the gap between the two interacting wall particles change relative to the initially set pectin layer gap, this stiff force acts as a one-to-one contact force between the two participating wall particles.

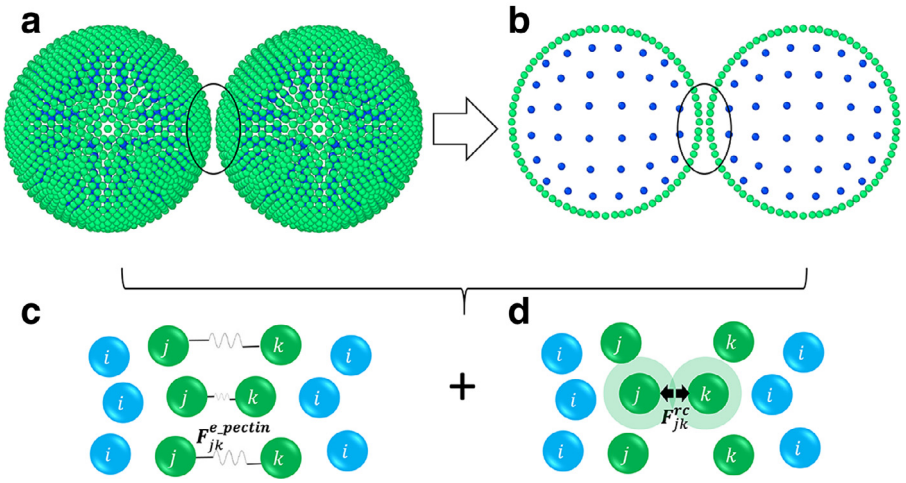

Fig. 4. Computational methodology for aggregating cells and defining the cell-cell interactions: (a) spherical initial cell geometry used in the small tissue arrangement with a positive middle lamella gap; (b) depiction of interacting cell wall particle pairs; (c) stiff forces in the pectin layer; (d) LJ repulsion forces in the pectin layer (green (j & k): wall particles; blue (i): fluid particles). (For interpretation of the references to colour in this figure legend, the reader is referred to the web version of this article.)

The pectin layer stiff force on any wall particle j due to its initial neighbouring particle k on the wall of the neighbouring cell is defined as,

$$\boldsymbol{F}_{jk}^{e\_pectin} = -k_{pectin}\Delta\boldsymbol{x}_{jk} \tag{3}$$

where, k_{pectin} is the pectin layer stiffness and $\Delta\boldsymbol{x}_{jk}$ is the difference between the current and the initial gap between the respective wall particle pair. This stiff force physically tries to maintain the gap between the wall particle pair equal to the initially set pectin layer thickness. In addition, it is the force acting in between cells when they try to separate from each other.

When the interacting cells come close to each other, a repulsion force is created due to the pectin layer stiffness to separate the cells and maintain the initially set pectin layer gap. The intensity of this stiff force is usually insufficient to fully prevent the cells from penetrating each other. Hence, an additional LJ type force has been used for this purpose by Van Liedekerke et al. [20]. When implementing this LJ force field, the initial particle gap (r_0) used for LJ force calculations is set to half of the initial pectin layer gap (see Fig. 4(d)). Accordingly, when the particle k approaches particle j, until their gap is equal to half of the initial pectin layer gap, only the pectin layer stiff force acts on the two particles to separate them. However, when the two particles come further closer (beyond half of the pectin layer thickness), the LJ forces start to act, which is stronger compared to the pectin layer repulsive stiff force and help effectively separate the two approaching particles. The cell-cell repulsive LJ forces are defined as:

$$\boldsymbol{F}_{jk}^{rc} = \sum_{j} f_{jk}^{rc}\boldsymbol{x}_{jk} \tag{4}$$

Where, f_{jk}^{rc} is the strength of the LJ force field and $\boldsymbol{x}_{jk}$ is the position vector of particle j relative to particle k. f_{jk}^{rc} is defined similar to that of the cell wall LJ force field. To effectively prevent cell-cell penetrations, f_{jk}^{rc} is set comparatively higher than that of the other LJ force fields used in the cell wall model. Using these two force interactions, individual cells are aggregated and the tissue model is developed. The following Section describes how the model was computationally set up and evolved.

2.5. Computational implementation and evolution of the model during simulations

In arranging the 3-D particle scheme for cells and aggregates, COMSOL Multiphysics software was used to define and fine-tune the initial particle placement of the cells due to the flexibility offered by the software. The computational evolution and boundary treatment of the cell-aggregate model was implemented in an equivalent manner as in our previously published work [16]. In addition, further details regarding turgor pressure treatment and steady state achievement could be found there. The aforementioned single cell model was used as a basic building block for the cell aggregates as discussed in Section 2.4 using the model parameters given in Table 1. For each individual cell aggregated, common values were used for the osmotic potential, turgor pressure and initial moisture content, and they were allowed to undergo parallel inflation processes according to the time evolution cycle explained above. In order to quantify the cellular deformations in the model

Table 1
Physical property values used for the 3-D single cell numerical model, representing an apple cell.

Parameter	Value	Reference
Initial cell radius [μm]	75	[42]
Cell wall shear modulus (G) [MPa]	18	[43]
Initial thickness of the cell wall (t) [μm]	6	[43]
Initial cell fluid mass [kg]	1.767×10^{-9}	Set ([22])
Initial cell wall mass [kg]	1.767×10^{-10}	Set ([22])
Cell wall damping ratio (γ) [Ns/m]	5×10^{-6}	Set([22])
Cell fluid viscosity (μ) [Pas]	0.1	Set ([19,20])
Initial SPH smoothing length (h_0) [μm]	6.8	Set ([17,19,22])
Turgor pressure of fresh cell (P_T) [kPa]	200	[32]
Osmotic potential of fresh cell ($-\pi$) [kPa]	- 200	Equal to - P_T ([19,22])
Cell wall permeability (L_P) [m^2s/N]	2.5×10^{-6}	[31]
Cell fluid compression modulus(K) [MPa]	20	Set ([22])
Number of fluid particles (N_f)	3082	Set
Number of wall particles (N_w)	2067	Set
LJ contact strength for attraction forces (f_0^a) (Nm^{-1})	1×10^{-11}	Set
LJ contact strength for repulsion forces (f_0^r) (Nm^{-1})	5×10^{-12}	Set
Cell wall bending stiffness (k_b) [$Nmrad^{-1}$]	1.0×10^{-10}	Set ([25])
Cell wall contraction force coefficient (k_{wc}) [Nm^{-1}]	1.0×10^{4}	Set ([25])
Pectin layer stiffness (k_{pectin}) (Nm^{-1})	1	Set
Pectin layer thickness (t_p) [μm]	8	Set
LJ contact strength for cell–cell repulsions ($f^{cc}{}_0$)	1.0×10^{-10}	Set ([28])

predictions, four geometrical parameters were employed: normalise cell area (A), diameter[1](D), and roundness[2] (R) similar to [16]. These parameters were normalised (A/A_0, D/D_0, R/R_0) by dividing the current value of the parameter by initial value at the fresh cell state (X_0, A_0, D_0 and R_0) to enable a better comparison.

3. Results and discussion

3.1. Selecting the optimum particle resolution of a cell model

The performance of a given SPH-based computational model is mainly influenced by the particle resolution (i.e. the number of particles used to represent and discretise the problem domain) [19,22,33]. To study the influence of particle resolution towards the performance of the computational model developed in this study, a series of numerical studies were carried out on a fully inflated turgid cell model. The particle resolution was varied to four different levels. Higher numerical accuracy and computational efficiency were targeted in determining the optimum particle resolution. The percentage model consistency error[3] (*MCE*) [16] was taken as a measure of the numerical accuracy while the overall computational time was considered as a measure of the computational efficiency of the model.

MCE value and the computational time for the simulations corresponding to each particle resolution have been graphed in Fig. 5. The results exhibit increasing numerical accuracy with the increasing particle resolution, which is demonstrated by the generally reducing *MCE* value. The particle resolution which contains 2067 wall particles and 3082 fluid particles demonstrates the highest degree of computational accuracy through maintaining a *MCE* value of 0.6%. However, when the particle resolution is increased beyond this point, there is a trend of decreasing computational accuracy as seen in Fig. 5 where there is a higher *MCE* value for the particle resolution which contains 2516 wall particles and 3859 fluid particles. This could be due to the propagation of numerical errors in the computational scheme throughout the simulations. The computational efficiency decreases with the increasing particle resolution, as clearly evident from the increasing computational times as seen in Fig. 5. This is due to the increasing number of computations arising with the increased particle numbers. Considering the trade-off between the computational accuracy and computational efficiency, the particle resolution with 2067 wall particles and 3082 fluid particles was decided to be the optimum particle scheme since it allows a high accuracy at a favourable computational cost.

3.2. Sensitivity analyses

3.2.1. The influence of wall contraction forces (WC) and wall bending forces (WB) on the morphological predictions of the model

The effects of the wall contraction forces (WC) and wall bending forces (WB) on the morphological behaviour of this cellular drying model are shown in Fig. 6 aiming for a qualitative comparison. Fig. 6(a) depicts deformation of the original state of the single cell model which accounts for both the wall contraction forces (WC) and wall bending forces (WB). Fig.

[1] $\sqrt{4A/\pi}$.
[2] $4\pi A/P^2$.
[3] $Model\ Consistency\ Error\ (MCE) = (model\ hoop\ force - theoretical\ hoop\ force)/theoretical\ hoop\ force$.

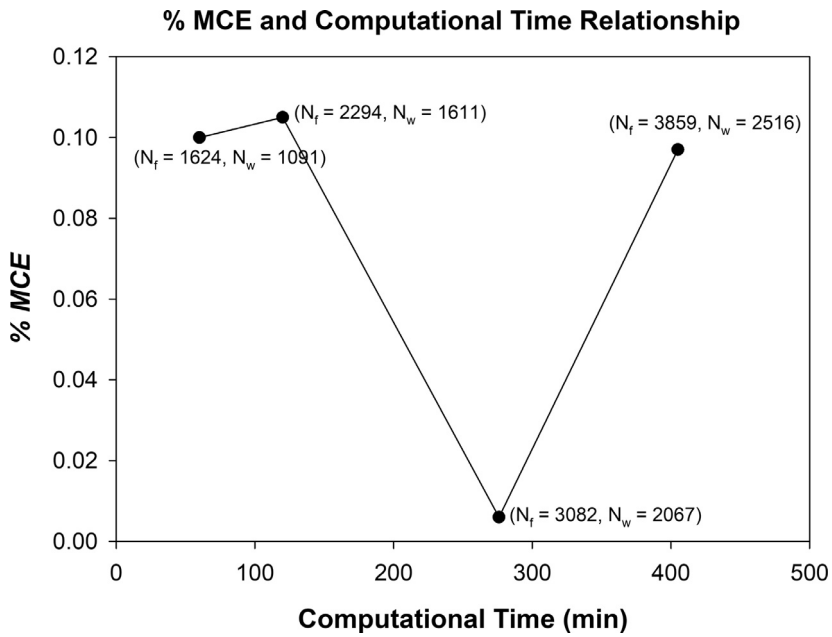

Fig. 5. The percentage model consistency error (*MCE*) values and the computational times corresponding to different particle resolutions (N_f– number of fluid particles and N_w – number of wall particles).

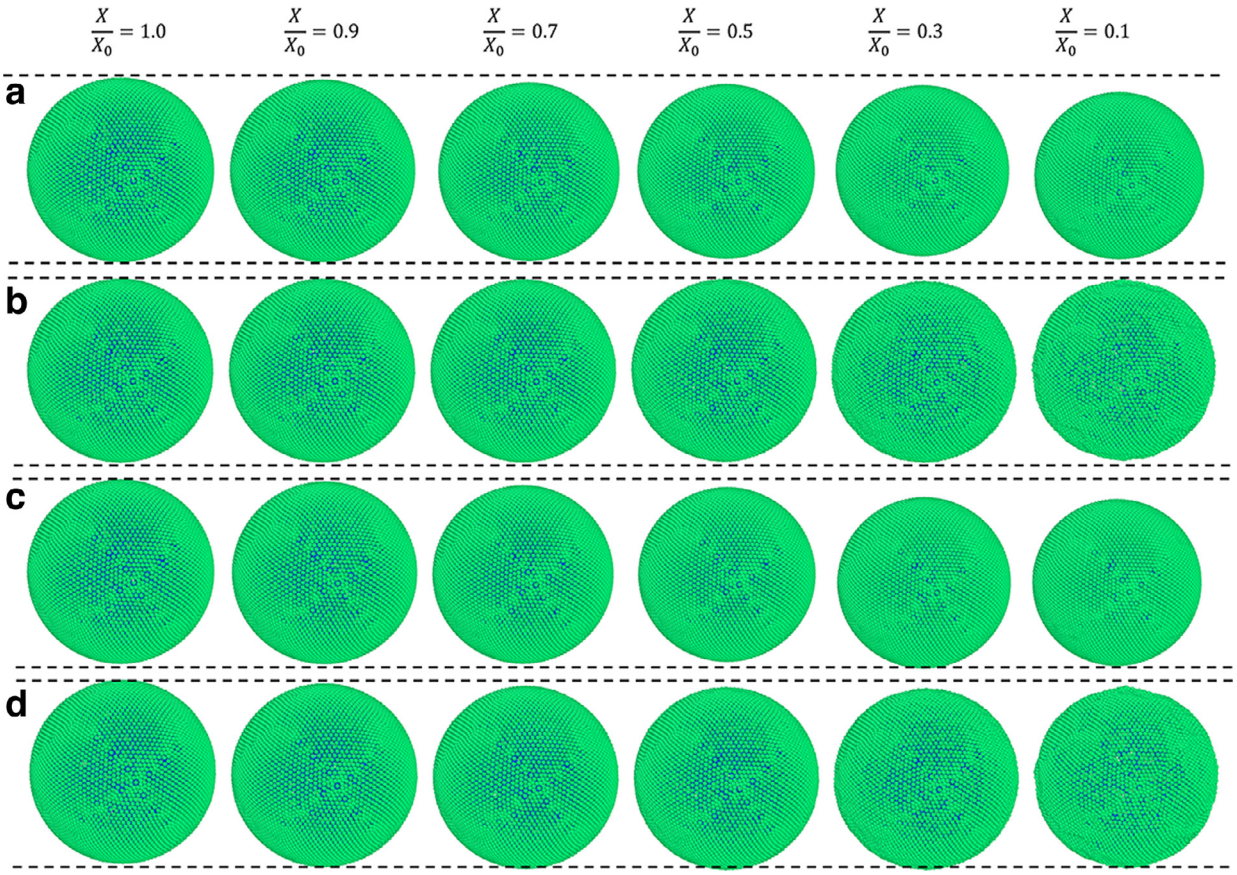

Fig. 6. Influence of the cell wall contraction forces (WC) and wall bending forces (WB) on the morphological behaviour of the model: (a) with WC and WB; (b) without WC; (c) without WB; (d) without WC and WB.

6(b) corresponds to the model behaviour in the absence of wall contraction forces (WC). It could be observed that cell shrinkage reduces when the wall contraction forces (WC) are omitted (see $X/X_0 \leq 0.3$ dryness states). In addition, the cell wall surface demonstrates a higher degree of surface wrinkling when the wall contraction forces (WC) are absent. This highlights that there is a significant impact of the wall contraction forces (WC) on the cellular morphological description and consequently, it will affect the alignment between model outcomes and corresponding experimental results.

Fig. 6(c) shows the model behaviour in the absence of wall bending forces (WB). As seen from this figure, the morphological behaviour of the cell model is not significantly affected in the absence of wall bending forces (WB). It is similar to the original behaviour of the cell model shown in Fig. 6(a). This implies that the presence of the wall bending forces (WB) is not critical for the model predictions to be valid when compared with the experimental findings. However, it should be noted that inclusion of wall bending forces (WB) is important in order to account for the local bending and wrinkling resistance of the plant cell walls which is observed in real plant cellular structures. It is a necessary phenomenon to be included in this analysis for the sake of depicting and analysing the biomechanical aspects present in the real food-plant cellular structures during drying [22].

Fig. 6(d) shows the model behaviour when both the wall contraction forces (WC) and wall bending forces (WB) are not accounted for. Cell model behaviour during drying in this state demonstrates a similar behaviour to the wall contraction forces (WC) absent state, which is shown in Fig. 6(b). The shrinkage is relatively lower compared to both Fig. 6(a) and (c) while the cell wall surface exhibits localised surface wrinkling. According to Fig. 6(b) and (c), the reduction of shrinkage may be due to the absence of wall contraction forces (WC). Fig. 6 provides an example for the capabilities of a coupled SPH-CG approach to approximate the morphological behaviour of real plant cellular structure in terms of shrinkage and wrinkling behaviour. It could be qualitatively observed that these are in close alignment with the experimental findings reported in our previously published experimental investigations [44] on similar types of cells.

In order to complement the above qualitative analysis, a quantitative study on the influence of wall contraction forces (WC) and wall bending forces (WB) was also carried out using the normalised geometrical parameters such as: normalised cell area (A/A_0) Feret diameter (D/D_0) and roundness (R/R_0). The consequent results are shown in Fig. 7. From Fig. 7(a)–(c), it could be observed that the area and diameter variation during drying in the absence of wall contraction forces (WC), significantly deviates from the experimentally observed behaviour. The magnitude of this discrepancy becomes larger with increasing degree of dryness. The omission of wall bending forces (WB) does not make the morphological behaviour of the model deviate further from the experimental findings. These quantifications re-confirm the conclusions drawn in the qualitative analysis above.

3.2.2. Model sensitivity to the SPH smoothing length (h)

The particle number in the SPH influence domain of fluid particles largely depends on the smoothing length [17]. The number of particles in the influence domain of a given SPH particle determines the degree of smoothing applied in that particular SPH computational scheme as a whole. This is directly correlated to the accuracy, stability and the computational cost of the entire modelling and simulation framework. To investigate the influence of the smoothing length variations on the model predictions, a sensitivity analysis was conducted. The smoothing length value (h) was varied during separate simulations and the model predictions were compared against each other as well as against the experimental findings. Percentage model consistency error (*MCE*) and the agreement of the simulation results with the experimental findings were taken as decisive parameters in determining the applicability of different smoothing lengths. Accordingly, the variation of *MCE* with the smoothing length (h) was studied and the results obtained are graphically presented in Fig. 8. It could be observed that at a smoothing length of 6.8 µm, *MCE* reaches a minimum of 0.6% leading to the highest accuracy in this SPH-CG computational scheme. When the smoothing length is above 6.8 µm, *MCE* increases gradually. This is an expected outcome which aligns with the fundamentals of SPH. When the smoothing length is varied beyond the optimum value, critical details of the particle or their local properties are smoothed-out leading to a lower accuracy. This numerical phenomenon is commonly reported in existing SPH literature [17]. For the smoothing length values below 6.8 µm, the consistency error increases in a steeper manner, mainly due to the lack of SPH influence domain particles to exert sufficient influences on a given fluid particle [17]. These results suggest that the optimum value for smoothing length is 6.8 µm for the single-cell model.

The post-processed results of the fully inflated cells (as sectioned side-views) at a selected set of smoothing lengths are visualised in Fig. 9. There is a significant change in the cell fluid morphological behaviour as shown. The fluid particle scheme exhibits a highly distributed nature at lower smoothing length values (e.g. 5.6 µm) while it tends to be relatively confined at higher smoothing length values (e.g. 8.8 µm). The higher number of particle-particle interactions at the high end of the smoothing length spectrum could be arising due to the increased number of influence domain particles.

3.2.3. Model sensitivity for mass transfer characteristics

Drying could be simply described as the transfer of water out of a given material. The mass transfer characteristics of such a system have a significant impact on the morphological behaviour during drying. For instance, the permeability of the cell wall affects the deformations of the cells while they undergo drying. Analogously, it could be observed that the mass transfer parameters have a substantial impact on the behaviour of the developed model in this study. The accuracy of the model predictions and the stability of the simulations depend on the selected mass transfer parameters. The cell wall permeability (or the cell wall hydrodynamic conductivity- L_P) could be given as an important parameter governing the mass transfer in this modelling and simulation scheme. To study the sensitivity of the model predictions with respect to the

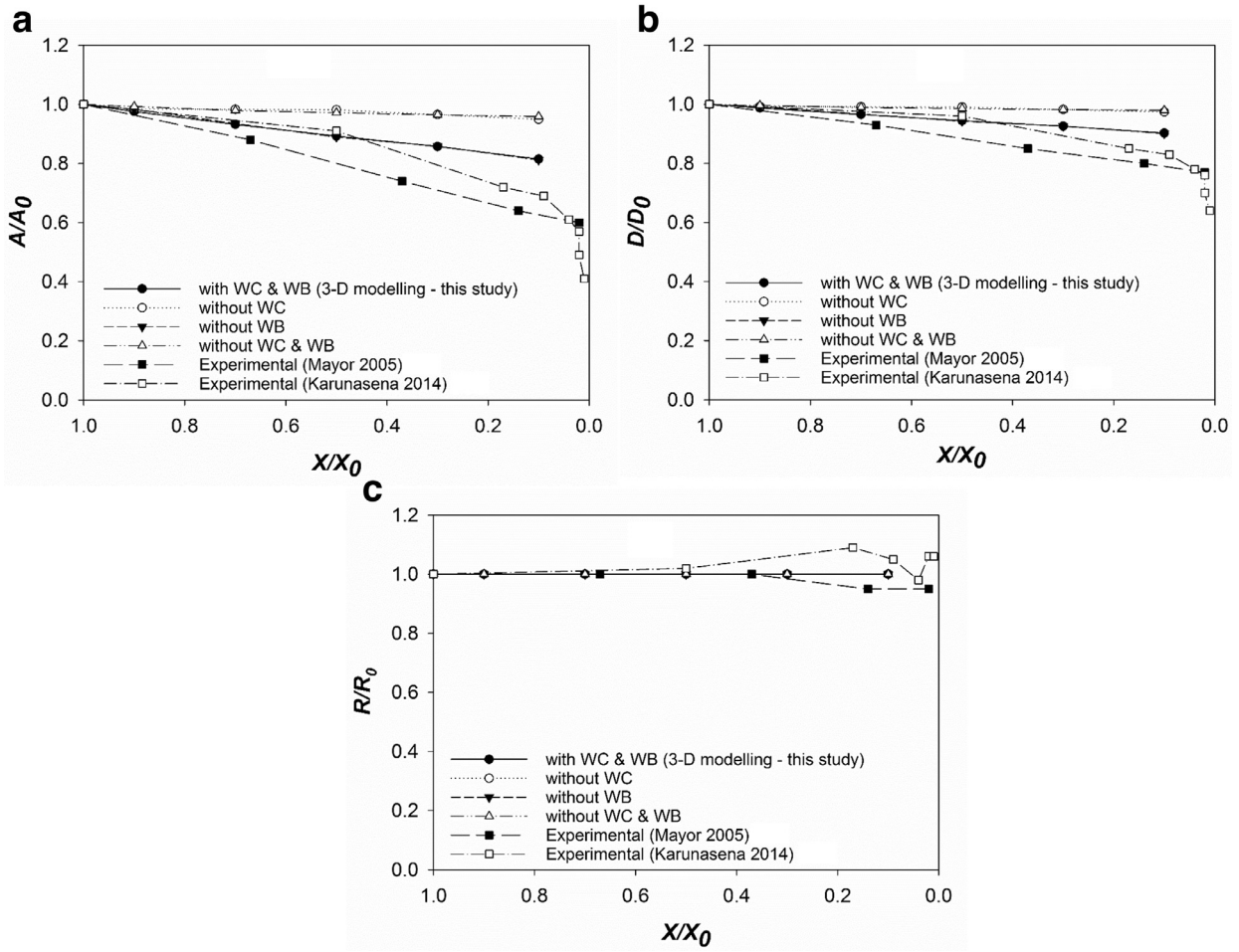

Fig. 7. Influence of the cell wall contraction forces (WC) and wall bending forces (WB) on the morphological behaviour of the model: (a) variation of normalised cell area (A/A_0) with the normalised moisture content (X/X_0); (b) variation of normalised cell diameter (D/D_0) with the normalised moisture content (X/X_0); (c) variation of normalised cell roundness (R/R_0) with the normalised moisture content (X/X_0).

Table 2
Different cell wall permeability (L_P) values and the resulting percentage model consistency error (MCE) values.

Permeability (L_P) (m^2 N^{-1} s)	% model consistency error (MCE)
2.5×10^{-5}	5.0
2.5×10^{-6}	0.6
2.5×10^{-7}	38.7
2.5×10^{-8}	83.4
2.5×10^{-9}	290.8
2.5×10^{-10}	342.6

magnitude of L_P, a series of simulations were executed by varying L_P. The resulting cell fluid mass variations with simulation time and MCE were observed. The final values of MCE for each of the L_P values were determined as given in Table 2. The cell fluid mass variation with simulation time is graphically shown in Fig. 10 and corresponding cell-models are visualised in Fig. 11 for a qualitative comparison.

It is noteworthy that the initial settling time or only the inflation stage of the single-cell models have been considered in this sensitivity analysis. The mass transfer characteristics of the system will influence the inflation process (during inflation) and the shrinkage (during drying) in equivalent ways as similar mass transfer characteristics and equation of state (EOS) are used for both the scenarios. Additionally, the method of assigning the end values of turgor pressure and osmotic potential are similar in both the cases. These are critical factors that govern the shrinkage behaviour of the cell during inflation and shrinkage. Therefore, it could be suggested that it is possible to deduce the results for the drying stage of the model by looking at the behaviour of the inflation. It should be mentioned here that for relatively higher values of L_P (i.e. $L_P \geq 2.5 \times 10^{-4}$

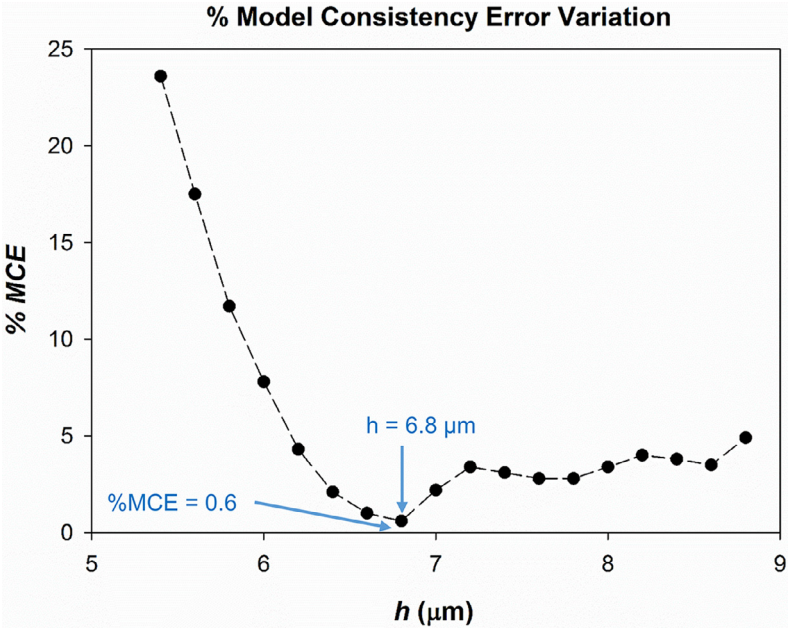

Fig. 8. Variation of the percentage model consistency error (*MCE*) with the smoothing length (*h*) of the SPH-CG computational scheme for a single-cell model.

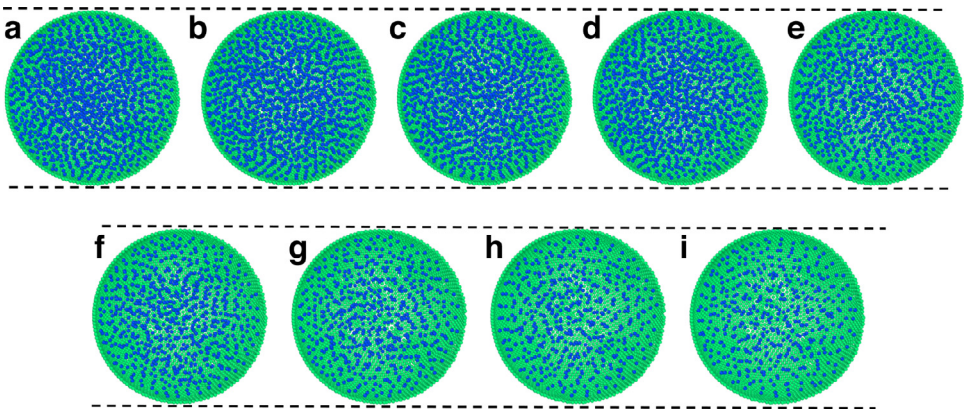

Fig. 9. Sectioned side-views of simulated cells at fully inflated state for different smoothing lengths (h) values: (a) 5.6 μm, (b) 6.0 μm, (c) 6.4 μm, (d) 6.8 μm (optimum/current study), (e) 7.2 μm, (f) 7.6 μm, (g) 8.0 μm, (h) 8.4 μm and (i) 8.8 μm, (green: wall particles, blue: fluid particles). (For interpretation of the references to colour in this figure legend, the reader is referred to the web version of this article.)

m^2N^{-1} s), the model became computationally unstable during the simulations. In terms of numerical modelling, this means that the corresponding value could be avoided.

According to the results, it is implied that at L_P values from 2.5×10^{-6} to 2.5×10^{-5} m^2N^{-1} s were leading to much higher mass transfer rates. This eventually results in higher fluid mass increments as observed in Fig. 11. The values of L_P below 2.5×10^{-7} m^2N^{-1} s lead to relatively very low mass transfer rates and eventually lower fluid mass increments. Therefore, such values could not be considered as favourable because those lead to higher computational times for achieving a given amount of fluid mass increment which is inefficient (similar for fluid mass losses in a drying scenario). Therefore, the values of 2.5×10^{-5} m^2N^{-1} s and 2.5×10^{-6} m^2N^{-1} s can be regarded as favourable for the cell model.

This is clearly visible from the qualitative results given in Fig. 11 where the cells corresponding to L_P values such as 2.5×10^{-5} m^2N^{-1} s and 2.5×10^{-6} m^2N^{-1} s are fully inflated with more uniform fluid particle distributions while the other cells are only partially inflated with poor fluid particle distributions. Ideally, an L_P value of 2.5×10^{-5} m^2N^{-1} s would be more favourable in terms of computational time as it leads to a rapid settlement of the cell than 2.5×10^{-6} m^2N^{-1} s. Nevertheless, *MCE* in the simulation outcomes corresponding to $L_P = 2.5 \times 10^{-5} m^2N^{-1}s$ is much higher compared to the model predictions at $L_P = 2.5 \times 10^{-6} m^2N^{-1}s$ (see Table 2). Therefore, an L_P value of 2.5×10^{-6} m^2N^{-1} s could be concluded as more suitable as it leads to more accurate computations while being computationally efficient at the same time.

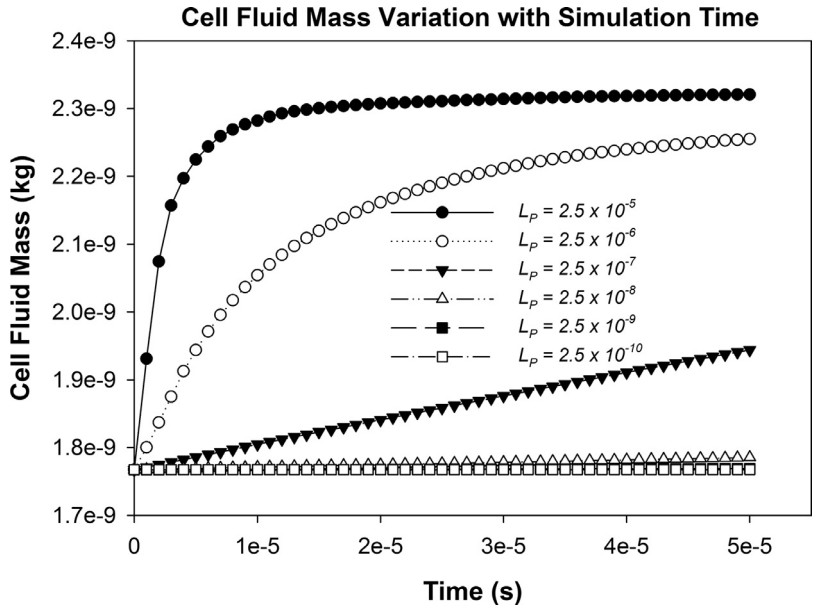

Fig. 10. Variation of cell fluid mass at different cell wall permeability (L_P) values.

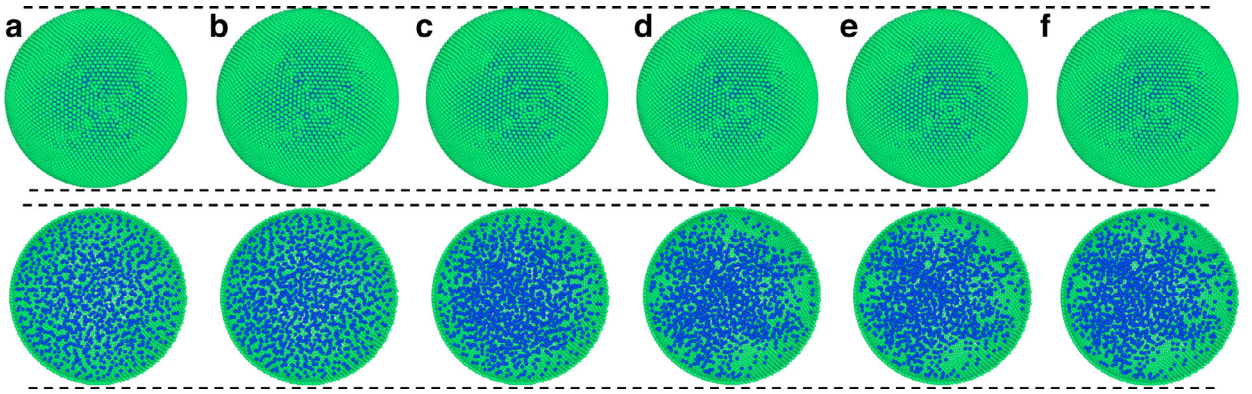

Fig. 11. Effects of different cell wall permeability (L_P) values on the inflation of the single-cell model: (a) $L_P = 2.5 \times 10^{-5}$; (b) $L_P = 2.5 \times 10^{-6}$; (c) $L_P = 2.5 \times 10^{-7}$; (d) $L_P = 2.5 \times 10^{-8}$; (e) $L_P = 2.5 \times 10^{-9}$ and (f) $L_P = 2.5 \times 10^{-10}$; (green: wall particles, blue: fluid particles). (For interpretation of the references to colour in this figure legend, the reader is referred to the web version of this article.)

3.3. Simulating morphological behaviour of cell aggregates during drying

For cell aggregates, a number of cell dryness states were simulated from a fresh state ($X/X_0 = 1.0$ and $P_T = 200$ kPa) to a critically dried state ($X/X_0 = 0.1$ and $P_T = 20$ kPa). This wide range of moisture content reduction achieved in this study is a key advantage compared to the previously reported comparable grid-based computational models [16,45]. Highlighting the novel work implemented in the current study, in Fig. 12, 3-D SPH-CG cell aggregate model predictions have been presented for all dryness states for single-cell, two-cell aggregate and four-cell aggregate arrangements respectively. It can be observed that the cell size gradually decreases as drying progresses for cell aggregate models. The simulation outcomes were then compared with experimental results on apple cells [44] in a qualitative manner before investigating the agreement in a quantitative manner. Such comparisons indicate that the cell models undergo shrinkage during drying leading to surface wrinkling and varied cellular interactions.

Next, the simulation outcomes for the dried cell model for single-cell, two-cell and four-cell systems were quantified through three parameters: cell area (A), Feret diameter (D) and roundness (R). The results were compared against experimental results from two sources in literature for apple tissues [46,47]. Comparison results for the normalised area is shown in Fig. 13. There is a reasonable agreement between the model outcomes and experimental results for the single cell model as well as cell aggregate models. Although the number of cells aggregated here is relatively small (i.e. two and four), there is still a laudable agreement with the relevant experimental findings due to the generic shrinkage behaviour of real plant cells being accurately captured by the meshfree-based SPH-CG cell aggregate model developed in this study. However, when

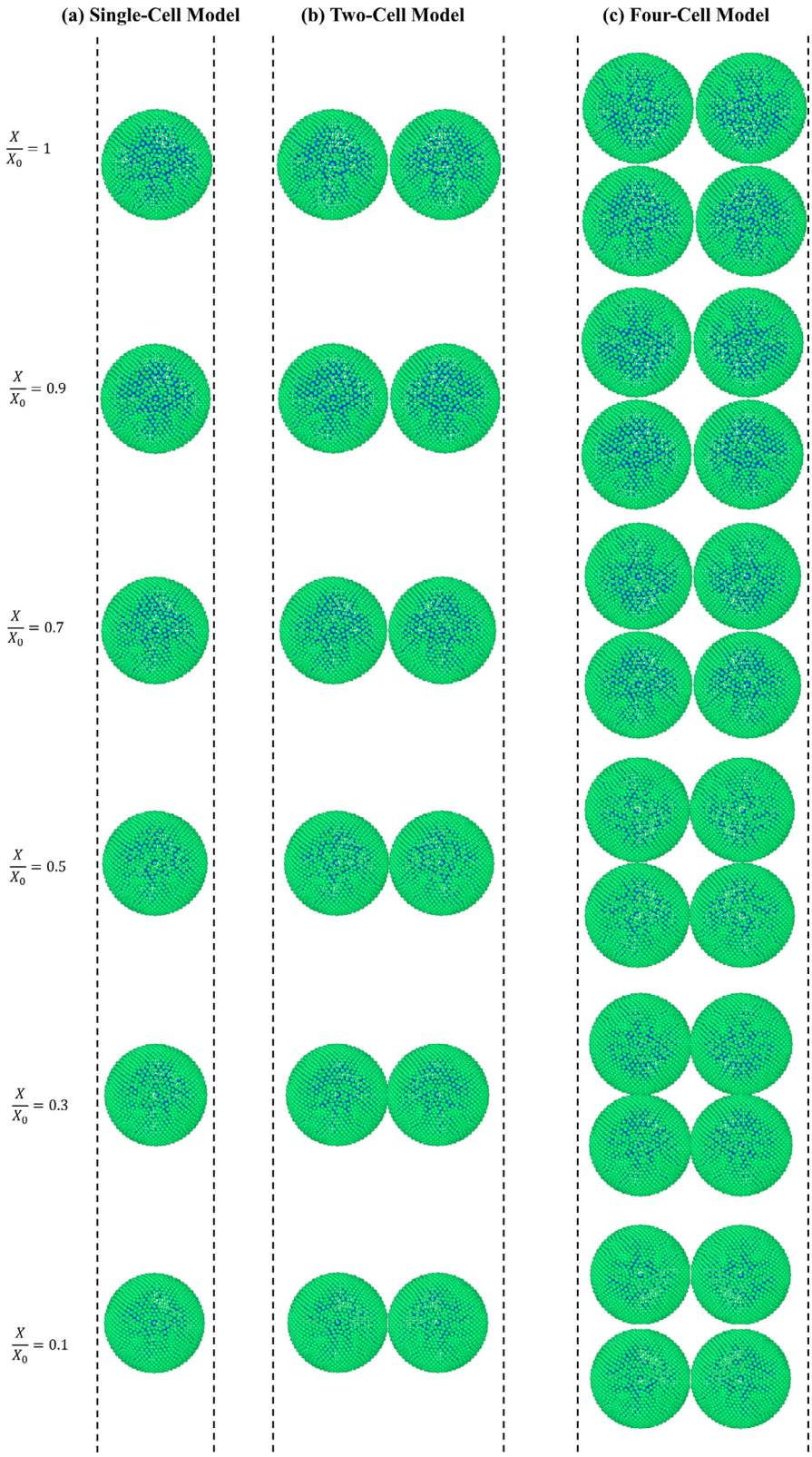

Fig. 12. 3-D SPHD-CG model predictions for (a) single-cell model (b) two-cell model and (c) four-cell model (green: wall particles, blue: fluid particles). (For interpretation of the references to colour in this figure legend, the reader is referred to the web version of this article.)

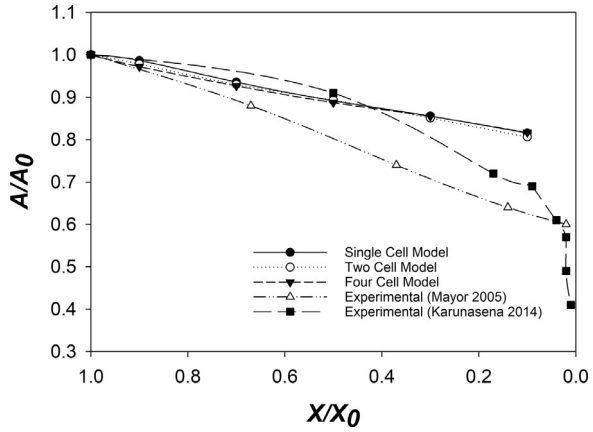

Fig. 13. Comparison of the variation of normalised cell area (A/A_0) with normalised moisture content (X/X_0) for cell aggregate models.

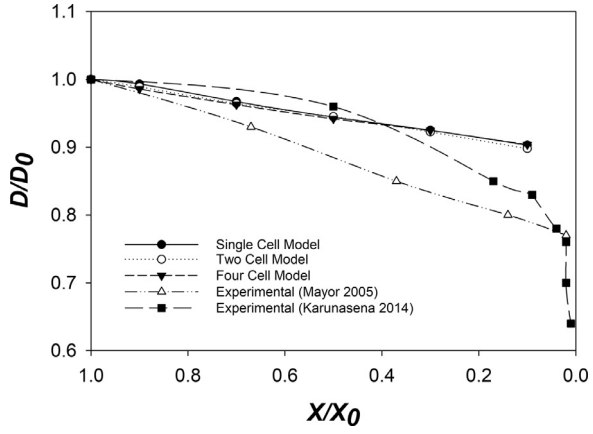

Fig. 14. Comparison of the variation of normalised cell diameter (D/D_0) with normalised moisture content (X/X_0) for cell aggregate models.

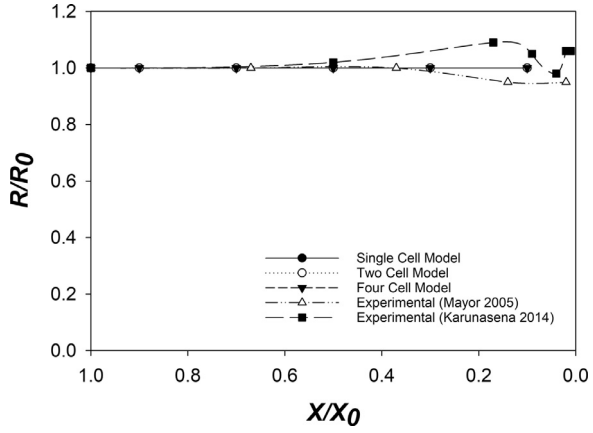

Fig. 15. Comparison of the variation of normalised roundness (R/R_0) with normalised moisture content (X/X_0) for cell aggregate models.

reaching the extremely dried conditions ($X/X_0 \leq 0.3$), differences between model predictions and experimental outcomes increase to a considerable level. There is a similar trend for the normalised diameter (D/D_0) variation as seen in Fig. 14. The agreement between the computational outcomes and experimental results is highly evident in the higher moisture contents. At extremely dried conditions, these discrepancies add up to a significant degree of mismatch for the single-cell model as well as for the two-cell and four-cell aggregate models. However, the overall agreement is still significantly favourable.

When the cell roundness (R/R_0) is considered for cell aggregate models, the experimental findings show a consistent value which is close to unity throughout the whole moisture domain for two-cell and four-cell aggregate models. As per Fig. 15, the roundness predicted by cell aggregate models in this study follows a comparable behaviour throughout the whole moisture content range. At the moment, the single-cell model and small cell aggregates are not fully capable of mimicking the behaviour of real cellular structures despite being able to estimate with an acceptable level of accuracy. It should be noted that this study is the first 3-D meshfree-based plant cell aggregate drying model reported, and the main intention was to demonstrate the fundamental computational mechanics associated with the cellular morphological alterations for small scale aggregates. As described above, notable discrepancies exist especially when it comes to extremely dried conditions (i.e. $X/X_0 \leq 0.3$). Based on the results of this study, it is predicted that more complicated physical and mathematical formulations and computational algorithms will need to be integrated into the current SPH-CG numerical framework to approximate such extreme and irregular morphological behaviours in the cellular structure. Additionally, aggregating larger numbers of cells to make up larger tissues could improve the degree of accuracy in the approximations implemented through this computational modelling approach. Considering the strengths of the current 3-D meshfree-based computational approach as seen in this study, the authors predict that the ability of a larger tissue model to closely describe the irregular and highly deformed nature of the cellular structure even at extremely dried circumstances will be higher.

4. Conclusion

Small plant cell aggregates were simulated using a three dimensional (3-D) Smoothed Particle Hydrodynamics (SPH) and Coarse-Grained (CG) coupled computational approach to predict the morphological behaviour during drying. It is noteworthy that this study is the first 3-D meshfree-based plant cell aggregate drying model reported which is a novel contribution compared to existing research from other researchers and our own work (e.g. [16]). In this investigation, the main intention was to demonstrate the fundamental computational mechanics associated with cellular morphological alterations for small scale plant cell aggregates. The model predictions of these cell aggregate models have been compared qualitatively and quantitatively through comparisons with experimental findings. The results show that the shrinkage and wrinkling behaviour of the cell aggregate models are in reasonable agreement with real cellular structures. It has been found that the agreement between the cell aggregate model predictions and the experimental findings are closer in the high and medium moisture content values ($X/X_0 \geq 0.3$), than highly dried stages ($X/X_0 < 0.3$). In addition, a study has been carried out to determine the optimum particle resolution of a cell model considering both computational accuracy and computational efficiency. This revealed that the particle resolution which contained 2067 wall particles and 3082 fluid particles was the optimum particle scheme since it allowed a very high accuracy at a favourable computational cost.

A sensitivity analysis was conducted to understand the influence of wall contraction forces and wall bending forces used in the cell wall morphological description. According to the results, it was concluded that wall contraction forces have a larger influence towards the morphological behaviour of the developed cell models than wall bending forces. Another sensitivity analysis was conducted with the objective of investigating the behaviour of the model towards varying SPH smoothing length (h) implying that a smoothing length value of 6.8 μm is optimum for maintaining the best computational accuracy. Also, a sensitivity analysis on the mass transfer characteristics showed that the cell wall permeability value (L_P) of 2.5×10^{-6} m^2N^{-1} s provides a stable solution to the numerical model while maintaining a high computational efficiency.

In future work, more complicated physical/mathematical formulations and computational algorithms will need to be integrated into the current SPH-CG numerical framework to approximate more extreme and irregular morphological behaviours in the cellular structure. Larger tissue models could also have the potential to closely describe the irregular and highly deformed nature of the cellular structure even at extremely dried circumstances. In addition, incorporating temperature variation effects into the current SPH-CG mathematical modelling framework will also be an interesting development in terms of more closely mimicking the true drying operations and their morphological implications. It would also be a critical phenomenon when it comes to approximating different types of drying processes and determining the nutritional value of dried food plant materials such as fruit and vegetables. Furthermore, there is a high potential for the developed SPH-CG numerical computational approach to be utilised in the 3-D multiscale level in order to predict the bulk scale deformations and mechanics of food plant tissues during drying.

Acknowledgements

The financial support from the ARC Discovery Project (DP150100828) and ARC Linkage Project (LP150100737) is acknowledged. We kindly acknowledge the High Performance Computing (HPC) facilities and Central Analytical Research Facility (CARF) of Queensland University of Technology (QUT), Brisbane, Queensland, Australia; the financial support provided by the Chemistry, Physics and Mechanical Engineering (CPME) scholarship provided by the Science and Engineering Faculty (SEF), QUT. In addition, we extend our acknowledgement for the support provided by the Faculty of Engineering, University of Moratuwa, Sri Lanka and the Faculty of Engineering, University of Ruhuna, Sri Lanka.

References

[1] J.D. Anderson, J. Wendt, Computational Fluid Dynamics, Springer, 1995.
[2] Q. Gao, R. Pitt, Mechanics of parenchyma tissue based on cell orientation and microstructure, Trans. ASAE 34 (1991).

[3] H.X. Zhu, J.R. Melrose, A mechanics model for the compression of plant and vegetative tissues, J. Theor. Biol. 221 (2003) 89–101.
[4] M. Abera, S. Fanta, P. Verboven, Q. Ho, J. Carmeliet, B. Nicolai, Virtual fruit tissue generation based on cell growth modelling, Food Bioprocess Technol. 6 (2013) 859–869.
[5] H. Honda, H. Yamanaka, M. Dan-Sohkawa, A computer simulation of geometrical configurations during cell division, J. Theor. Biol. 106 (1984) 423–435.
[6] Y. Ishimoto, Y. Morishita, Bubbly vertex dynamics: A dynamical and geometrical model for epithelial tissues with curved cell shapes, Phys. Rev. E 90 (2014) 052711.
[7] G.R. Liu, Meshfree Methods: Moving Beyond the Finite Element Method, CRC press, 2010.
[8] J. Loodts, E. Tijskens, C. Wei, E.L.S. Vanstreels, B. Nicolaï, H. Ramon, Micromechanics: Simulating the elastic behavior of onion epidermis tissue, J. Text. Stud. 37 (2006) 16–34.
[9] S.B. Nilsson, C.H. Hertz, S. Falk, On the relation between turgor pressure and tissue rigidity. II, Physiol. Plant. 11 (1958) 818–837.
[10] P. Pathmanathan, J. Cooper, A. Fletcher, G. Mirams, P. Murray, J. Osborne, J. Pitt-Francis, A. Walter, S.J. Chapman, A computational study of discrete mechanical tissue models, Phys. Biol. 6 (2009) 036001.
[11] A.E. Smith, K.E. Moxham, A.P. J, On uniquely determining cell–wall material properties with the compression experiment, Chem. Eng. Sci. 53 (1998) 3913–3922.
[12] C.M. Rathnayaka, H.C.P. Karunasena, Y.T. Gu, L. Guan, W. Senadeera, Novel trends in numerical modelling of plant food tissues and their morphological changes during drying – a review, J. Food Eng. 194 (2017) 24–39.
[13] C.M. Rathnayaka, H.C.P. Karunasena, W. Senadeera, L. Guan, Y.T. Gu, Three-dimensional (3D) numerical modeling of morphogenesis in dehydrated fruits and vegetables, in: G. Chen (Ed.), Advances in Agricultural Machinery and Technologies Ed., CRC Press, Boca Raton, 2018, pp. 431–454.
[14] J.J. Monaghan, Smoothed particle hydrodynamics, Ann. Rev. Astron. Astrophys. 30 (1992) 543–574.
[15] M.B. Liu, G.R. Liu, Smoothed particle hydrodynamics (SPH): an overview and recent developments, Arch. Comput. Methods Eng. 17 (2010) 25–76.
[16] C.M. Rathnayaka, H.C.P. Karunasena, W. Senadeera, Y.T. Gu, Application of a coupled smoothed particle hydrodynamics (SPH) and coarse-grained (CG) numerical modelling approach to study three-dimensional (3-D) deformations of single cells of different food-plant materials during drying, Soft. Matter. 14 (2018) 2015–2031.
[17] G.R. Liu, M.B. Liu, Smoothed Particle Hydrodynamics: A Meshfree Particle Method, World Scientific, 2003.
[18] T. Belytschko, Y. Krongauz, D. Organ, M. Fleming, P. Krysl, Meshless methods: an overview and recent developments, Comput. Methods Appl. Mech. Eng. 139 (1996) 3–47.
[19] P. Van Liedekerke, P. Ghysels, E. Tijskens, G. Samaey, B. Smeedts, D. Roose, H. Ramon, A particle-based model to simulate the micromechanics of single-plant parenchyma cells and aggregates, Phys. Biol. 7 (2010) 026006.
[20] P. Van Liedekerke, P. Ghysels, E. Tijskens, G. Samaey, D. Roose, H. Ramon, Mechanisms of soft cellular tissue bruising. A particle based simulation approach, Soft. Matter. 7 (2011) 3580–3591.
[21] P. Van Liedekerke, E. Tijskens, H. Ramon, P. Ghysels, G. Samaey, D. Roose, Particle-based model to simulate the micromechanics of biological cells, Phys. Rev. E 81 (2010) 061906.
[22] H.C.P. Karunasena, W. Senadeera, Y.T. Gu, R.J. Brown, A coupled SPH-DEM model for micro-scale structural deformations of plant cells during drying, Appl. Math. Model. 38 (2014) 3781–3801.
[23] H.C.P. Karunasena, W. Senadeera, R.J. Brown, Y.T. Gu, Simulation of plant cell shrinkage during drying – a SPH–DEM approach, Eng. Anal. Bound. Elem. 44 (2014) 1–18.
[24] H.C.P. Karunasena, Y.T. Gu, R.J. Brown, W. Senadeera, Numerical investigation of plant tissue porosity and its influence on cellular level shrinkage during drying, Biosyst. Eng. 132 (2015) 71–87.
[25] H.C.P. Karunasena, R.J. Brown, Y.T. Gu, W. Senadeera, Application of meshfree methods to numerically simulate microscale deformations of different plant food materials during drying, J. Food Eng. 146 (2015) 209–226.
[26] H.C.P Karunasena, Y.T. Gu, R.J. Brown, W. Senadeera, Numerical investigation of case hardening of plant tissue during drying and its influence on the cellular-level shrinkage, Dry. Technol. 33 (2015) 713–734.
[27] H.C.P. Karunasena, W. Senadeera, R.J. Brown, Y.T. Gu, A meshfree model for plant tissue deformations during drying, ANZIAM J. 55 (2014) C110–C137.
[28] H.C.P. Karunasena, W. Senadeera, R.J. Brown, Y.T. Gu, A particle based model to simulate microscale morphological changes of plant tissues during drying, Soft. Matter. 10 (2014) 5249–5268.
[29] C.M. Rathnayaka, Meshfree-based numerical modelling of three-dimensional (3-D) microscale deformations of plant food cells during drying, 2017 Doctoral dissertation, Queensland University of Technology.
[30] C.M. Rathnayaka, H.C.P. Karunasena, Y.T. Gu, L. Guan, J. Banks, W. Senadeera, A 3-D meshfree numerical model to analyze cellular scale shrinkage of different categories of fruits and vegetables during drying, in: G.R. Liu, S. Li (Eds.), Proceedings of the 7th International Conference on Computational Methods, Scientech Publisher, Berkeley, CA, USA, 2016, pp. 1070–1080.
[31] L. Taiz, E. Zeiger, Plant Physiology, Sinauer Associates, New York, 2002.
[32] C. Wang, L. Wang, C. Thomas, Modelling the mechanical properties of single suspension-cultured tomato cells, Ann. Botany 93 (2004) 443–453.
[33] P.W. Cleary, J.J. Monaghan, Conduction modelling using smoothed particle hydrodynamics, J. Comput. Phys. 148 (1999) 227–264.
[34] J.J. Monaghan, Smoothed particle hydrodynamics, Rep. Progr. Phys. 68 (2005) 1703.
[35] P. Constantin, C. Foias, Navier–Stokes Equations, University of Chicago Press, 1988.
[36] R. Temam, Navier–Stokes Equations: Theory and Numerical Analysis, American Mathematical Soc., 2001.
[37] J.P. Morris, P.J. Fox, Y. Zhu, Modeling low Reynolds number incompressible flows using SPH, J. Comput. Phys. 136 (1997) 214–226.
[38] B. Fan, J.K. Maranas, Coarse-grained simulation of cellulose Iβ with application to long fibrils, Cellulose 22 (2015) 31–44.
[39] K. Lu, J.K. Maranas, S.T. Milner, Ion-mediated charge transport in ionomeric electrolytes, Soft. Matter. 12 (2016) 3943–3954.
[40] L. Petridis, H.M. O'Neill, M. Johnsen, B. Fan, R. Schulz, E. Mamontov, J. Maranas, P. Langan, J.C. Smith, Hydration control of the mechanical and dynamical properties of cellulose, Biomacromolecules 15 (2014) 4152–4159.
[41] B.A. Veytsman, D.J. Cosgrove, A model of cell wall expansion based on thermodynamics of polymer networks, Biophys. J. 75 (1998) 2240–2250.
[42] B.P. Hills, B. Remigereau, NMR studies of changes in subcellular water compartmentation in parenchyma apple tissue during drying and freezing, Int. J. Food Sci. Technol. 32 (1997) 51–61.
[43] N. Wu, M.J. Pitts, Development and validation of a finite element model of an apple fruit cell, Postharvest Biol. Technol. 16 (1999) 1–8.
[44] C.M. Rathnayaka, H.C.P. Karunasena, W. Senadeera, Y.T. Gu, Application of 3D imaging and analysis techniques for the study of food plant cellular deformations during drying, Dry. Technol. 36 (2018) 509–522.
[45] S.W. Fanta, M.K. Abera, W.A. Aregawi, Q.T. Ho, P. Verboven, J. Carmeliet, B.M. Nicolai, Microscale modeling of coupled water transport and mechanical deformation of fruit tissue during dehydration, J. Food Eng. 124 (2014) 86–96.
[46] H.C.P. Karunasena, P. Hesami, W. Senadeera, Y.T. Gu, R.J. Brown, A. Oloyede, Scanning electron microscopic study of microstructure of gala apples during hot air drying, Dry. Technol. 32 (2014) 455–468.
[47] L. Mayor, M. Silva, A. Sereno, Microstructural changes during drying of apple slices, Dry. Technol. 23 (2005) 2261–2276.